

RSC Advances



This is an *Accepted Manuscript*, which has been through the Royal Society of Chemistry peer review process and has been accepted for publication.

Accepted Manuscripts are published online shortly after acceptance, before technical editing, formatting and proof reading. Using this free service, authors can make their results available to the community, in citable form, before we publish the edited article. This *Accepted Manuscript* will be replaced by the edited, formatted and paginated article as soon as this is available.

You can find more information about *Accepted Manuscripts* in the [Information for Authors](#).

Please note that technical editing may introduce minor changes to the text and/or graphics, which may alter content. The journal's standard [Terms & Conditions](#) and the [Ethical guidelines](#) still apply. In no event shall the Royal Society of Chemistry be held responsible for any errors or omissions in this *Accepted Manuscript* or any consequences arising from the use of any information it contains.



Journal Name

ARTICLE

Received 00th January 20xx,
Accepted 00th January 20xx
DOI: 10.1039/x0xx00000x

www.rsc.org/

Dendrimer-based preparation and luminescence studies of SiO₂ fibers doping Eu³⁺ activator in interstitial sites

Jie Chen^a, Ye Sheng^a, Xiuqing Zhou^a, Murad M.A. Abualrejal^a, Meiqi Chang^a, Zhan Shi^b, Haifeng Zou^{*,a}

Luminescent one-dimensional Eu³⁺ doped SiO₂ fibers have been readily prepared by electrospinning method combined with a sol-gel process. In this work, polyvinylpyrrolidone (PVP) as a simple commercial dendrimer not only increased the viscosity of solution but also provided weak hydrogen bonds with silica, which was significant in improving the electrospinnability. The scanning electron microscopy (SEM) and transmission electron microscopy (TEM) showed that the as-obtained samples present fiber-like morphology with uniform size and the diameters of fibers became wider with the increase of Eu³⁺ concentration, from nanoscale to microscale. The X-ray diffraction (XRD), Fourier transform infrared spectroscopy (FT-IR) and X-ray photoelectron spectroscopy (XPS) indicated that Eu³⁺ activator ions have been doped into the interstitial sites of SiO₂ fibers through the electrostatic interaction, which would reduce the symmetry of SiO₂ framework. The photoluminescence (PL) properties include the diffuse reflectance, excitation and emission spectra indicated that the obtained SiO₂:Eu³⁺ fibers exhibited typical Eu³⁺ (⁵D₀₋₇F_J) red emission under ultraviolet excitation and the band energy was changed due to the doping of stable Eu³⁺ activator ions. Meanwhile, the concentration quenching effects and decay kinetics behaviors of SiO₂:Eu³⁺ fibers were investigated and the optimal doping concentration and the longest lifetime were both in the composition of 16 mol % Eu³⁺. In addition, the energy-dispersive X-ray spectrum (EDS), thermogravimetry differential thermal analysis (TG-DTA) and the formation mechanism were also displayed in order to better understand the work.

1. Introduction

As is well-known, inorganic luminescent materials include rare earth compounds and rare earth ions doped compounds have been extensively investigated and play a vital role in high-performance luminescent devices, cell imaging and other fluorescent displays fields based on their unique optical, electronic and chemical characteristics arising from their 4f electrons¹. Meanwhile, it has been recognized that particles size, morphology and arrangement have crucial influences on their luminescence properties. For example, the Gd₂O₃:Eu³⁺ oriented film showed much stronger emission intensity than irregular powders². The quantum efficiency values of Eu³⁺ ions in one-dimensional materials are higher than corresponding nanoparticles and bulk materials³. What's more, one-dimensional (1D) structures including fibers, wires and belts have attracted a great many interests because of their extensive applications in energy conversion and storage, supercapacitors and LEDs fields⁴. Based on these, it is significant to develop a facile and effective method to directly prepare the rare earth ions doped one-dimensional luminescent materials in nano/microscale with respect

to expand their applications in energy conversion and storage, supercapacitors and LEDs fields.

Electrospinning is known as a simple, convenient, cost-effective, and versatile technique to generate long fibers compared with other methods, such as chemical vapor deposition⁵, hydrothermal method⁶ and laser ablation⁷. What's more, the fibers prepared by electrospinning have good orientation, controllable morphology and the diameters are ranging from tens of nanometers up to micrometers by tuning the electrospun parameters. In general, the typical electrospinning procedure can be divided into three parts⁸: (1) The preparation of precursor solution of inorganic materials containing a polymer together; (2) Set up the parameters of electrospinning to prepare the polymer/inorganic composite fibers; (3) Calcination the composite fibers under high temperature to remove the polymer and obtain the desirable nano/microfibers. Dendrimer (such as PVP and PVA) in this process are used to control viscosity and serve as template to generate 1D structure. A schematic of the electrospinning equipment was shown in Scheme 1. Up to now, a variety of rare earth ions doped 1D phosphor fibers materials have been prepared using electrospinning technique, such as CeO₂⁹, GdVO₄¹⁰ and other metal oxide¹¹, which adding inorganic salt constituent into the precursor solutions directly. However, it is difficult to guarantee the smoothness, strength, toughness and ductility of the above fiber materials only with this kind of method¹². In order to solve this problem, sol-gel condensation reaction as an

^a College of Chemistry, Jilin University, Changchun 130012, PR China

^b State Key Laboratory of Inorganic Synthesis and Preparative Chemistry, College of Chemistry, Jilin University, Changchun 130012, PR China

*Corresponding author, Tel.: +86-431-85155275; Fax: +86-431-85155275

E-mail address: haifengzou0431@gmail.com

DOI: 10.1039/x0xx00000x

efficient way to produce IV oxide nanoparticles¹³ is thought to be a good choice to prepare precursor solutions and the concentration of rare earth ions in the host materials is easily controlled by adjusting the ratios of rare earth ions to IV oxide sol-gel precursors¹⁴. What's more, in terms of various host materials for rare earth ions, SiO₂ possesses multiple advantages including thermal stability, corrosion resistance, biocompatibility, efficient photoluminescence emission and a broad spectral transmission range¹⁵. Particularly, the 3D network structure of SiO₂ is not only conducive to protect and stabilize the rare earth ions inside, but also allow its optical properties to be detected from outside due to the high optical transparency of silica¹⁶. Meanwhile, this host material is also fully compatible with silica-based optical fiber industry and has been successfully employed to fabricate two-dimensional Er-doped film waveguides and amplifiers¹⁷. In addition, SiO₂ is a wide band gap semiconductor due to the presence of donor sites such as oxygen vacancies and self-trapped excitons¹⁸, which implies that electroluminescence also could be realized from the luminescent rare earth ions doped SiO₂ fibers. Therefore, a combination of electrospinning method with sol-gel process is one appealing route to obtain 1D rare earth ions doped silica phosphor fibers materials¹⁹, which can expand their applications in many fields, such as sensors, electronic and optical devices, catalyze and biology fields²⁰.

In this work, a large scale of one-dimensional Eu³⁺-doped SiO₂ fibers have been conventionally synthesized by electrospinning technique combined with a sol-gel process and the position of Eu³⁺ activator ions in SiO₂ matrix was discussed for the first time to our knowledge. The dendrimer PVP could be regarded as soft templates to crosslink silica molecule and its linear structure was assisted the orderly structure to form a fibrous morphology during electrospinning. Based on this, the formation mechanism of the Eu³⁺-doped SiO₂ fibers was investigated in detail. What is more important, we have proved that Eu³⁺ ions were efficiently doped into the interstitial sites of SiO₂ matrix and some weak interaction may exist, which have effects on the symmetry and band gap of SiO₂ matrix. Additionally, the photoluminescence property, concentration quenching effect and the decay kinetics behaviors of the samples have been systematically investigated by doping different amount of Eu³⁺ ions.

2. Experimental

2.1 Materials

Polyvinylpyrrolidone (PVP) ($M_w \approx 40,000$), absolute ethanol and acetic acid were bought from Beijing Chemical Reagents Co. Tetraethyl orthosilicate (TEOS) was bought from Internet Aladdin Reagent Database Inc. All materials were analytical grade reagents and needn't further purification. Eu(NO₃)₃ (1.0 M) solution was prepared by dissolving Eu₂O₃ (99.99%) powder in dilute HNO₃ solution under constantly heating and stirring.

2.2 Preparation

The SiO₂:Eu³⁺ fibers were prepared by electrospinning method.

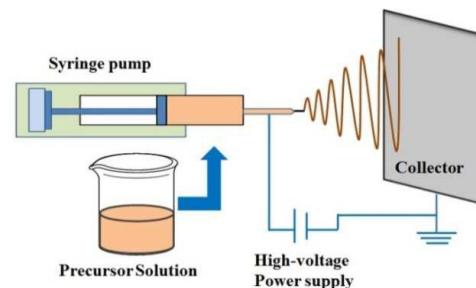
A typical electrospinning setup is consist of a syringe sump, a high-voltage power supply, a flat tip needle and a flat collector, as shown in scheme 1.

In the first step, 1.5g of TEOS and different amount of europium nitrate (the molar ratio of Eu/Si was 0.04, 0.08, 0.12, 0.16, 0.20 and 0.24) was mixed with 2ml ethanol and 3ml acetic acid, which acted as catalyst to hydrolyze the TEOS. After stirring 30min, 2g PVP was added into the solution, followed by magnetic stirring for ~2h to ensure all the PVP was dissolved, then the precursor solutions were obtained.

In the second step, the precursor solutions were loaded into plastic syringes equipped with 20 gauge stainless needles. The needle was connected with a high-voltage power supply to generate Dc voltages from -4KV to 16KV, sum up 20KV. A plate of Al₂O₃ foil as the collection screen was placed at a distance of 20cm from needle tip to collector. The electrospinning process was conducted in air. The as-prepared precursor fibers were left in air for several hours to make TEOS hydrolyzed completely. In order to reduce the presence of -OH and organic groups, which were responsible for the luminescence intensity and quenching, the precursor fibers were calcined in air atmosphere at 600°C for 2h.

2.3 Characterization

X-ray powder diffraction was measured by a Rigaku D/max-B II X-ray diffractometer with Cu K α radiation. The field emission scanning electron microscope (FESEM) images were observed by S-4800, Hitachi. Transmission electron microscopy (TEM) images were obtained with a JEM-2000EX TEM (acceleration voltage of 200 kV). The thermogravimetry differential thermal analysis (TG-DTA) was carried out on a Thermal Analysis instrument (SDT 2960, TA Instruments, New Castle, DE) with a heating rate of 10 °C/min. Fourier transform infrared (FT-IR) spectra were performed on a Perkin-Elmer 580B infrared spectrophotometer with the KBr pellet technique. Energy-dispersive spectroscopy (EDS) analysis was performed with an H JEOL JXA-840 EDX system attached to the SEM microscope. The X-ray photoelectronspectra (XPS) were taken using a VG ESCALAB 250 electronenergy spectrometer with Mg K α (1253.6 eV) as the X-ray excitation source. The reflection spectra were calibrated with the reflection of white BaSO₄ (reflection ~100%) in the wavelength region of 200-800 nm. The PL measurements were determined using Jobin Yvon FluoroMax-4 luminescence spectrophotometer equipped with a 150 W xenon lamp as the excitation source. All the measurements were performed at room temperature.



Scheme 1. The electrospinning setup

3. Results and Discussion

3.1 Thermal analysis

Fig.1 showed the thermal behavior of PVP/SiO₂:Eu³⁺ precursor fibers. From this Figure we could see that three weight loss stages were involved in TGA curve. The weight loss in the first stage between 50°C and 270°C was very slight, corresponding to 8.8%, which was caused by the loss of absorbed water and/or the evaporation of trapped solvent such as acetic acid and ethanol in the composite fibers. The second stage between 270°C to 380°C accompanied by a sharp exothermic peak located at 351°C in the DTA curve contributed to 38.9% weight loss, which due to the decomposition of organic components, such as the side-chain of PVP and residue TEOS. The third stage in the temperature change from 380°C to 600°C accompanied by a small exothermic peak near 490°C in the DTA curve, corresponding to 26.5% weight loss, which associated with the further degraded of polymer residues such as the main chain of PVP²¹. Above 600°C, TGA curve was unvaried, which indicated that water and all organic compounds in composite fibers were removed completely and pure Eu³⁺ doped SiO₂ fibers were obtained. The total weight loss of precursor fibers was 74.2%.

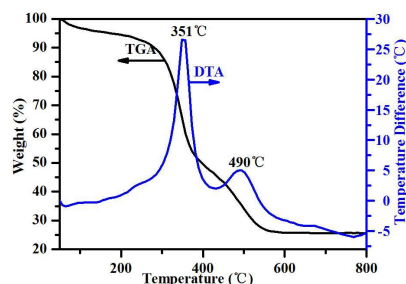


Fig.1 The TGA and DTA patterns of PVP/SiO₂:Eu³⁺ precursor fibers

3.2 Morphology and Structure properties

The SEM and TEM images of the as-formed PVP/SiO₂:xEu³⁺ (x=0.16) precursor fibers, as well as those samples annealed at 600 °C were shown in Fig.2. From this figure we could see the prepared samples consisted of uniform fibers, which distributed on the substrate with random orientation due to the bending instability related to the spinning jet. By comparing Fig.2 (a) and (b), it could be clearly observed that the calcination process didn't break the fiber-like morphology but the diameters of calcined SiO₂:Eu³⁺ fibers were greatly decreased because of the decomposition of the organic components (such as PVP) and the formation of inorganic phase. From the Fig 2(c) and (d) we could see that the obtained SiO₂:Eu³⁺ fibers were smooth and the diameters were about 660 nm.

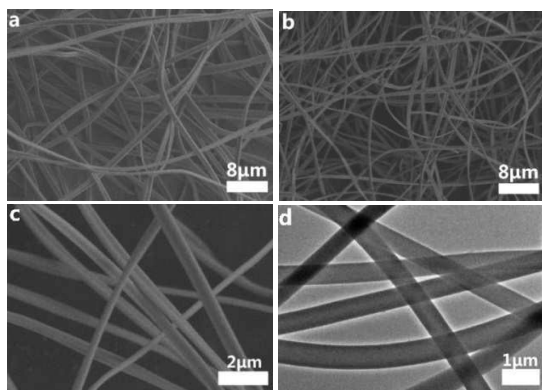


Fig.2 The SEM images of SiO₂:Eu³⁺ fibers (a) pre-calcination, (b) post-calcination of low-magnification, (c) high-magnification and (d) TEM image

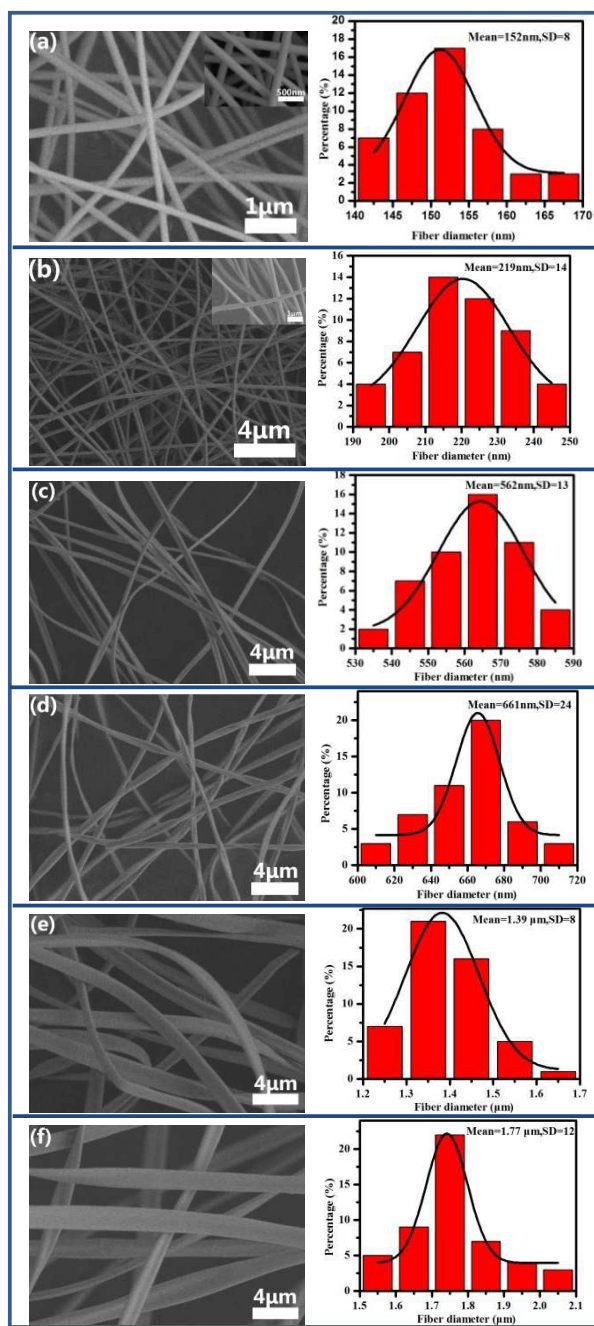


Fig.3 SEM images of SiO₂:xEu³⁺ fiber (a) x=0.04; (b) x=0.08; (c) x=0.12; (d) x=0.16; (e) x=0.20; (f) x=0.24.

The SEM images of the doping different Eu³⁺ concentrations SiO₂:Eu³⁺ fibers after calcination at 600°C were shown in Fig.3. From this figure it could be seen that with the increase of Eu³⁺ concentration, the diameters of fibers increased significantly, from nanoscale to microscale, which was attributed to the addition of high concentration Eu(NO₃)₃ solution. As we are known whether the fiber

morphology could be formed in electrospinning process was mainly decided by the volatility of solvents and the viscous force and surface tension of solution²². In general, the addition of high concentration solution could lead to the polymer solution to thicken. As shown in our work, with the increase of $\text{Eu}(\text{NO}_3)_3$ concentration we added into the mixture, the precursor solution containing PVP became more and more stickier, which gave rise to the enhance of viscous force and surface tension of precursor droplet²³. When the electrostatic force was not enough to overcome the viscous force and surface tension, the volatile components couldn't volatile out well, which resulting in the occur of conglutination phenomenon between fibers and obtained the coarser fiber diameter²⁴. The size distributions of the $\text{SiO}_2:\text{Eu}^{3+}$ fibers doping different Eu^{3+} concentrations were displayed in Fig.3, which measured from the SEM images by ImageJ.

The XRD patterns of $\text{SiO}_2:\text{xEu}^{3+}$ fibers ($x=0.0, 0.08, 0.16$) calcined at 600°C were presented in Fig.4. From this figure, it could be seen that only broad peaks could be observed at about $22-23^\circ$ in spite of Eu^{3+} concentration, which corresponding to the characteristic diffraction peak of amorphous SiO_2 ²⁵. Comparing with Fig.4 (a), (b) and (c), we could find that with the increase of Eu^{3+} concentration from $x=0.08$ to $x=0.16$, no detectable diffractions of Eu_2O_3 crystalline phase but amorphous SiO_2 . That was to say the global structure of samples didn't change when doping Eu^{3+} ions, while the diffraction peak intensity of samples obviously became weaker with the increasing Eu^{3+} concentration. The reason for this phenomenon may be attributed that the introduced Eu^{3+} ions occupied the vacancy of matrix SiO_2 , which has effects on the structural Si-O bond distance and/or Si-O-Si angles by strongly interacted with the O atoms²⁶, and then deformed the Si-O-Si network structure and reduced the symmetry of SiO_2 framework.

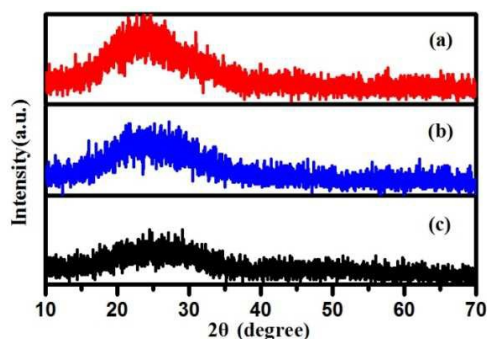


Fig.4 The XRD patterns of $\text{SiO}_2:\text{xEu}^{3+}$ fibers (a) $x=0.00$; (b) $x=0.08$; (c) $x=0.16$

In order to further investigate the structural changes in bonding of the precursor fiber and the $\text{SiO}_2:\text{Eu}^{3+}$ fiber, FT-IR spectra were applied. As seen from Fig.5, the broad peaks located at 3438cm^{-1} in three lines were all attributed to the $-\text{OH}$ symmetric vibration of absorbed water. For PVP and precursor fibers, the small peaks at 2951cm^{-1} and 1443cm^{-1} , the obvious peaks at 1656cm^{-1} and 1288cm^{-1} were attributed to the C-H bond, C=O bond and C-N bond vibrations of PVP, respectively²⁷. Comparing with the Fig.5 (i) and (ii), a new peak at 1151cm^{-1} was appeared in the precursor fibers, which was assigned to the vibration of Si-O-Si bond. After calcined

at 600°C , all the peaks related to PVP were disappeared and the vibration of Si-O-Si was prominent as shown in Fig.5 (iii). Additionally, it was interesting that the peak of Si-O-Si bond at 1151cm^{-1} in precursor fibers blue-shifted to 1072cm^{-1} after calcination, which indicated that there was weak hydrogen bond interaction may exist between PVP and SiO_2 molecules. In addition, the XRD results have revealed that the Eu^{3+} activator occupied in the SiO_2 matrix have an effect on the SiO_2 internal modes, which have been demonstrated that some interaction may exist between Eu^{3+} ions and O atoms²⁶. However, Eu^{3+} ions were hardly substituted with Si^{4+} due to the large difference on the ionic radius between Eu^{3+} and Si^{4+} (The ions radii of Si^{4+} and Eu^{3+} ion are 0.26 \AA and 1.087 \AA , respectively²⁸). So we conjectured that a pseudo-covalent bond is possibly formed at the interstitials sites of the SiO_2 matrix by the electrostatic interaction of $\text{Eu}^{3+}\dots[\text{SiO}_4]^{4-}\dots\text{Eu}^{3+}$ ²⁸ due to the special network structure of SiO_2 . That is to say that Eu^{3+} doped into non-crystalline interstitial regions of silica materials by interaction between Eu^{3+} ions and O ions sharing with SiO_4 tetrahedral units and caused the local symmetry of the SiO_2 matrix partially collapse, which was in agreement with the XRD results in Fig.4. Meanwhile, the FT-IR spectra have indicated that the organic molecules could be removed completely from the precursor fibers when the temperature was above 600°C and pure $\text{SiO}_2:\text{Eu}^{3+}$ fibers were obtained, which was consistent with TGA curve.

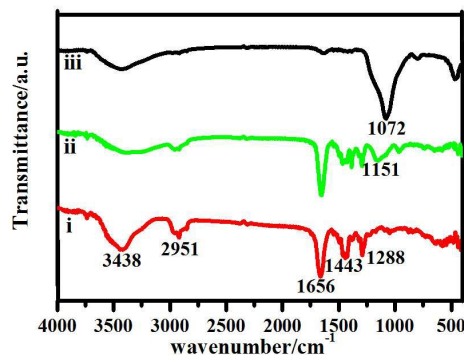


Fig.5 The FT-IR spectra of the samples (i) PVP; (ii) $\text{PVP}/\text{SiO}_2:\text{Eu}^{3+}$ precursor fibers; (iii) $\text{SiO}_2:\text{Eu}^{3+}$ fibers

3.3 Component analysis

The EDX spectra of $\text{PVP}/\text{SiO}_2:\text{Eu}^{3+}$ precursor fibers and $\text{SiO}_2:\text{Eu}^{3+}$ fibers were shown in Fig.6. The EDX characterization showed that four elements carbon (C), silicon (Si), oxygen (O) and europium (Eu) were existed in the precursor fibers, in which the atomic percent of C was very high. After calcination at 600°C , it could be seen only three elements, Si, O and Eu were existed in the $\text{SiO}_2:\text{Eu}^{3+}$ fibers, which meant that C element resulting from organic component (such as PVP) was completely removed after heat treatment and pure $\text{SiO}_2:\text{Eu}^{3+}$ fibers were obtained. The element-mapping images described the distribution of Si, O and Eu elements in $\text{SiO}_2:\text{Eu}^{3+}$ fibers by mapping the same region as the SEM image, which clearly indicated that Si, O and Eu atoms were homogeneously distributed in the $\text{SiO}_2:\text{Eu}^{3+}$ fibers. All the results above demonstrated that the luminescent one-dimensional Eu^{3+} doped SiO_2 fibers were prepared successfully.

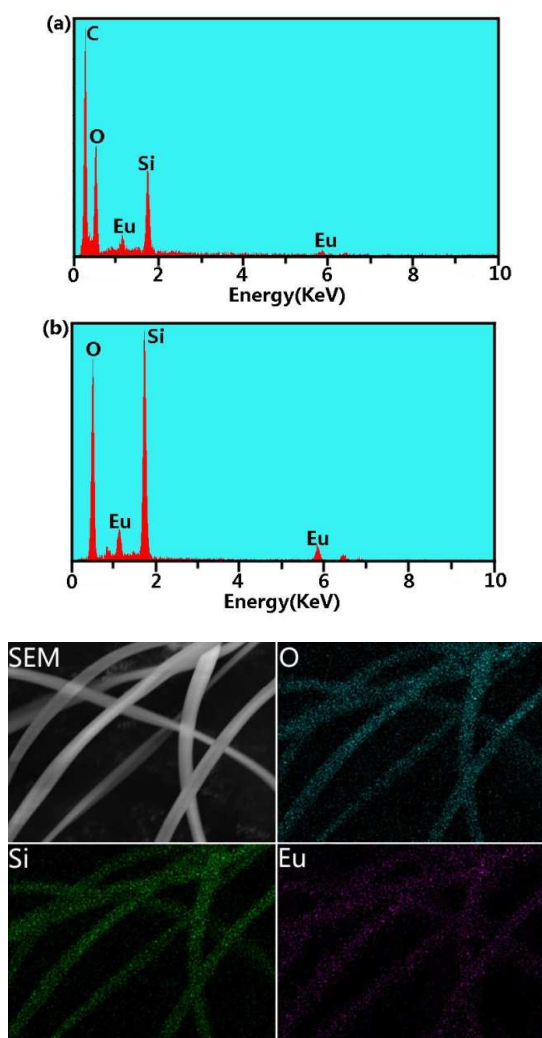


Fig.6 The EDX spectra of PVP/SiO₂:Eu³⁺ precursor fiber (a); SiO₂:Eu³⁺ fibers (b) and elemental mapping of SiO₂:Eu³⁺ fibers

In order to further investigate the chemical components and charge state of SiO₂:Eu³⁺ fibers, XPS analysis were performed (Fig.7). All peaks in the wide-scan XPS spectra could be well ascribed to Eu 3d, Eu 4d, O 1s, Si 2s, Si 2p and C 1s (introduced by the CO₂ in air absorbed on the substrate), respectively, which was good in agreement with the EDX spectra. As shown in high-resolution XPS spectra, with the increase of Eu³⁺ concentration in SiO₂:xEu³⁺ fibers (x=0.00, 0.08, 0.16), the Si (2p) peak blue shifted from 103.6 eV in pure SiO₂ to 103.5 eV and 102.8 eV, as well as the O (1s) peak blue shifted from 533.0 eV to 532.9 eV and 532.5 eV, which indicated the change of bonding way in SiO₂ matrix due to the doping of Eu³⁺ ions. Comparing with pure SiO₂, two new bands at 136.9 eV and 142.5 eV were belonged to Eu 4d_{5/2} and Eu 4d_{3/2}, which were in good agreement with the value of Eu³⁺ spin-orbital splitting of 5.6 eV²⁸. The same results were shown in Eu 3d spectra, two new intense peaks around 1134.9 eV and 1165.2 eV were assigned to the Eu 3d_{5/2} and Eu 3d_{3/2}, respectively. In addition, we found that the values of Eu 3d and Eu 4d in SiO₂ fibers were a little different with those in Eu₂O₃, which were 1134.2eV and 135.0eV for

Eu 3d_{5/2} and Eu 4d_{5/2} peaks. These different binding energy were due to the change of chemical environment of Eu element²⁹, which indicated that Eu³⁺ ions have been effectively doped into the SiO₂ fibers by some interaction rather than simply being mixed in the form of Eu₂O₃.

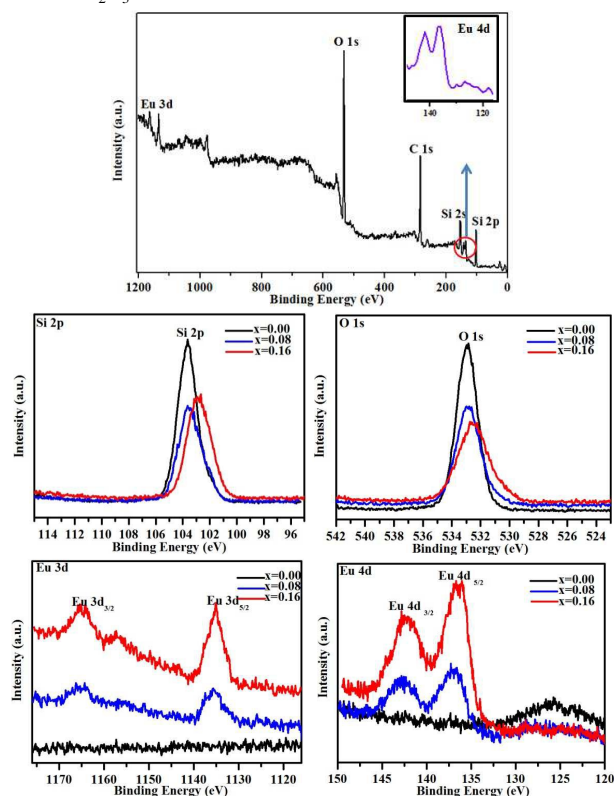
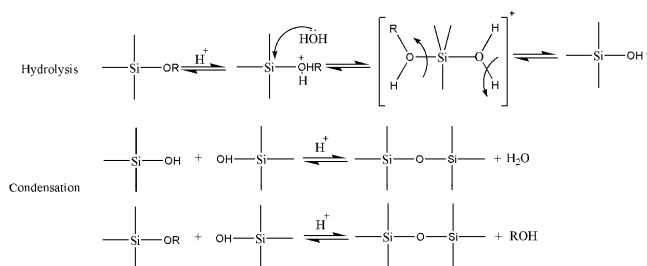


Fig.7 Wide-scan XPS spectra and high-resolution Si (2p), O (1s), Eu (3d) and Eu (4d) XPS spectra of SiO₂:Eu³⁺ fibers

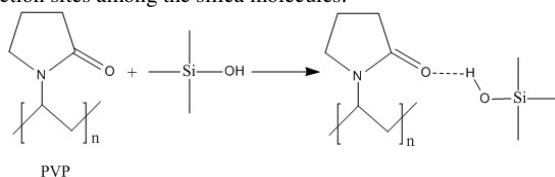
3.4 Formation mechanism

According to the characteristic analysis results mentioned above, we speculated that dendrimer PVP played an important role in the formation of SiO₂:Eu³⁺ fibers. The driving force in this self-assembly process was mainly because of the hydrogen bond interaction between SiO₂ molecular and PVP template, which could be completely removed by annealing process. Based on these, we speculated the mechanism of this reaction as shown in Fig.8.

First, TEOS molecules experienced a series of hydrolysis and condensation reactions after acetic acid was added into the system and formed Si-O-Si bond network structure with a byproduct of ethanol. And Eu³⁺ ions were incorporated into the clearance sites through the pseudo-covalent bond (Eu³⁺...[SiO₄]⁴⁻...Eu³⁺). It should be noted that TEOS could be fiercely hydrolyzed under much water, so we kept the sum of volume of water and Eu(NO₃)₃ solution to be constant. Acetic acid as catalyst in this system helped to promote the hydrolysis of TEOS and silica sol was formed completely after stirring for 2h.



Then dendrimer PVP was added to assist spinning by tuning the viscoelastic properties of silica sol-gel through the hydrogen bond between the OH groups on the surface of silica sol and the carbonyl groups of the PVP³⁰. After stirring for several hours, all PVP were dissolved and connected around the silica sol molecules. The final result of these crosslinking processes was the formation of larger composite gel consisted of SiO₂-PVP supramolecular molecules. The linear structure of PVP also helped the supramolecular arrange orderly and form a fibrous morphology during electrospinning and it also could be regarded as soft templates, which were located at the junction sites among the silica molecules.



Finally, the PVP and other volatile (such as ethanol, acetic acid and residual water, TEOS) were removed from the obtained composite electrospun fibers after calcination at high temperature (600°C in this system), while the fibers morphology of the inorganic framework remains. Then pure SiO₂:Eu³⁺ fibers were obtained.

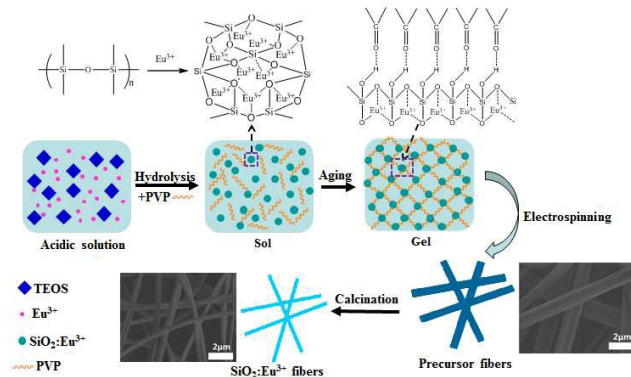


Fig.8 The formation mechanism of SiO₂:Eu³⁺ fibers

3.5 Photoluminescence properties

The photoluminescence properties of the SiO₂:Eu³⁺ fibers after calcination at 600 °C for 2h were investigated by the diffuse reflectance, excitation and emission spectra and the decay kinetics behaviors.

The reflectance spectra of SiO₂:xEu³⁺ (x=0.00, 0.12, 0.16) fibers were presented in Fig.9. As we could see in Fig.9 (a), a strong drop in reflection in the UV range below 300nm was corresponding to the valence-to-conduction band transition of SiO₂ host. In order to better understand the influences of doping Eu³⁺ ions, the absorption spectra

were obtained from the reflection spectra according to the Kubelka-Munk function³¹:

$$F(R) = (1 - R)^2 / 2R = K / S \quad (1)$$

Where R, K and S are the reflection, the absorption coefficient and the scattering coefficient, respectively. The absorption spectrum (K/S) of SiO₂:xEu³⁺ (x=0.00, 0.12, 0.16) fibers derived with the Kubelka-Munk function was shown in Fig.9 (b). For pure SiO₂, only a sharp absorption band with a peak center at about 227nm and its optical band gap was calculated to be about 4.8 eV (i.e., 257nm), which was closed to the reported value of 4.24 eV for pure SiO₂³². From Fig.9 (b), it could be clearly seen that the absorption edges showed an apparent red shift with the increase of Eu³⁺ ions concentration, which arising from the contribution of the new valence created by Eu³⁺ doping. In order to shed light on the reason of this red shift, several factors should be considered, such as doping effects, variations of SiO₂ host structure and so on. So far, a great many work has been revealed that the aliovalent doping can modify the symmetry and defect characteristics of host materials to modulate the band gap no matter doped on the surface or vacancy³³. And with the doping of Eu³⁺ ions, the structure occurred expansion, neighboring atoms were apart from each other, which would weakened the bonds and decreased the overlap between the orbitals of neighboring atoms³⁴.

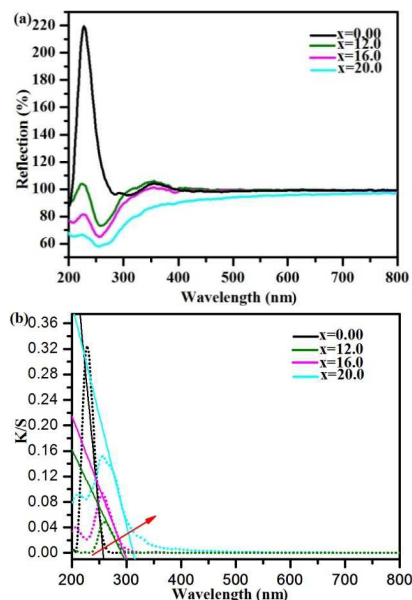


Fig.9 Diffuse reflection spectra of SiO₂:Eu³⁺ fibers

The excitation spectrum of the SiO₂:Eu³⁺ fibers was obtained by monitoring the emission of the ⁵D₀→⁷F₂ transition of Eu³⁺ at 613nm. As shown in Figure.10 (a), it contained several narrow peaks between 300 and 550nm corresponding to the f-f transitions of Eu³⁺ ions. Among all the peaks the maximum absorption peak was located at around 393nm attributed to the ground state ⁷F₀ to the excited ⁵L₆ state transition of intra-4f⁶ electron of Eu³⁺ ions²⁶.

As shown in Figure.10 (b), the emission spectra of SiO₂:Eu³⁺ fibers present the characteristic emission peaks of Eu³⁺ ions under the excitation at 393nm, which was corresponding to the intra-4f

transition of Eu^{3+} from metastable orbital singlet state $^5\text{D}_0$ to spin-orbital states of $^7\text{F}_J$ ($J = 0, 1, 2, 3, 4$)^{35,36}. Among all the peaks in the emission spectra between 500nm to 750nm, the strongest emission peak located at 613nm was attributed to the $^5\text{D}_0 \rightarrow ^7\text{F}_2$ transition, other peaks were attributed to the transitions of $^5\text{D}_0 \rightarrow ^7\text{F}_0$ (around 576nm), $^5\text{D}_0 \rightarrow ^7\text{F}_1$ (around 590nm), $^5\text{D}_0 \rightarrow ^7\text{F}_3$ (around 651nm) and $^5\text{D}_0 \rightarrow ^7\text{F}_4$ (around 701nm), which were shielded by the outer orbitals of 5S^2 and 5P^6 ^[26]. The photoluminescence of the $\text{SiO}_2:\text{Eu}^{3+}$ fibers was mainly attributed to the $^5\text{D}_0 \rightarrow ^7\text{F}_1$ and $^5\text{D}_0 \rightarrow ^7\text{F}_2$ peaks, and the $^5\text{D}_0 \rightarrow ^7\text{F}_2$ peak was dominant because of the hypersensitive forced electric dipole transition.

The luminescence intensity of $\text{SiO}_2:\text{Eu}^{3+}$ fibers was depended on the doping concentration of Eu^{3+} activator ions. In order to obtain the optimum luminescence intensity, we prepared the $\text{SiO}_2:\text{xEu}^{3+}$ fibers with different doping concentrations of Eu^{3+} ions and their luminescence intensities were displayed in Fig 11 (a). As we can see with the increase of Eu^{3+} concentration, the luminescence intensity enhanced due to the more and more luminescent centers, and the maximum emission intensity was obtained at a Eu^{3+} ions doping concentration of 16 mol %. When exceeding this critical concentration, the luminescence intensity of $\text{SiO}_2:\text{xEu}^{3+}$ fibers would gradually decrease, which was so-called concentration quenching effect³⁷. This was mainly due to the cluster of activators at high concentration would lead to the energy transfer by cross-relaxation between Eu^{3+} ions in the $\text{SiO}_2:\text{xEu}^{3+}$ fibers. For most of rare-earth activators, the concentration quenching effect was ascribed to the non-radiative energy transfer from rare-earth ions to nearby quenching centers, which usually through the exchange interaction and multipole-multipole interaction³⁸. At the same time, other non-radioactive processes such as energy transfer to hydroxyl ions and the defects in silica also could contribute to the luminescence quenching effects. From the results discussed above, it could be deduced that the optimum doping concentration of Eu^{3+} was $x=0.16$ in $\text{SiO}_2:\text{xEu}^{3+}$ fibers, which meaning the concentration quenching effect was occurred above the concentration of 16 mol % Eu^{3+} .

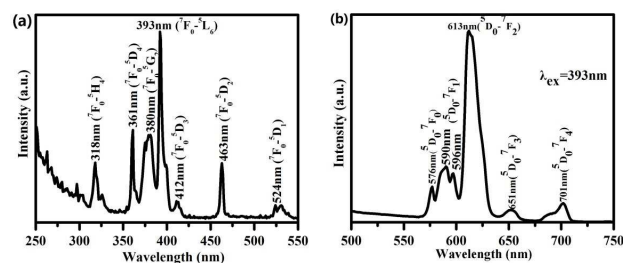


Fig.10 the excitation (a) and emission (b) spectra of $\text{SiO}_2:\text{Eu}^{3+}$ fibers

The decay kinetics behaviors of Eu^{3+} in $\text{SiO}_2:\text{xEu}^{3+}$ fibers were investigated. The lifetime decay curves for the $^5\text{D}_0 \rightarrow ^7\text{F}_2$ transition of Eu^{3+} (613nm) at different concentration were measured at room temperature under excitation at 393nm. As illustrated in Fig.11 (b), the decay curves for the $^5\text{D}_0 \rightarrow ^7\text{F}_2$ transition of Eu^{3+} in all samples could be fitted well by a double exponential function³⁹:

$$I(t) = I_0 + A_1 \exp\left(-\frac{t}{\tau_1}\right) + A_2 \exp\left(-\frac{t}{\tau_2}\right) \quad (2)$$

Where I and I_0 are the luminescence intensities at time t and 0, A_1 and A_2 are constants, t is the time, and τ_1 and τ_2 are the decay times

for the exponential components. As we know, the rare earth ions have two types in nanophosphors: one is at the surface and the other is in the “bulk”^{40, 41}. Same as this one-dimensional luminescent $\text{SiO}_2:\text{Eu}^{3+}$ fibers, two different luminous centers of Eu^{3+} activator ions existed in fibers, one was located at the disorder position on the surface of fibers, such as the defects sites; the other was located at the order sites in the inner of fibers, such as the network structure of SiO_2 . Therefore, the lifetime (τ) of Eu^{3+} in $\text{SiO}_2:\text{xEu}^{3+}$ fibers the lifetime was the average lifetime of the above two kinds of lifetime values and can be calculated by the below function:

$$\tau = (A_1 \tau_1^2 + A_2 \tau_2^2) / (A_1 \tau_1 + A_2 \tau_2) \quad (3)$$

Thus the average lifetimes of Eu^{3+} in $\text{SiO}_2:\text{xEu}^{3+}$ fibers ($x=0.04, 0.08, 0.12, 0.16, 0.20, 0.24$) could be determined to be 0.19, 0.27, 0.37, 0.43, 0.20, 0.13 ms, respectively. As seen in Fig.11 (b), with the increase of the Eu^{3+} content, the lifetime values of $\text{SiO}_2:\text{xEu}^{3+}$ fibers gradually extended until up to $x=0.16$, then tended to decrease. The variation tendency of decay lifetime sequence was consisted with the luminescence intensity of samples. That means both the strongest luminescence intensity and longest lifetime value were at $x=0.16$ in $\text{SiO}_2:\text{xEu}^{3+}$ fibers. As we all know that the luminescence intensity was proportional to radiative transition probability, while the decay lifetime was the inverse of the sum of the radiative transition and the non-radiative transition probability. Therefore, the non-radiative transition probability of Eu^{3+} from the $^5\text{D}_0$ energy level in the $\text{SiO}_2:\text{xEu}^{3+}$ fibers was small due to the decrease of surface defects⁴².

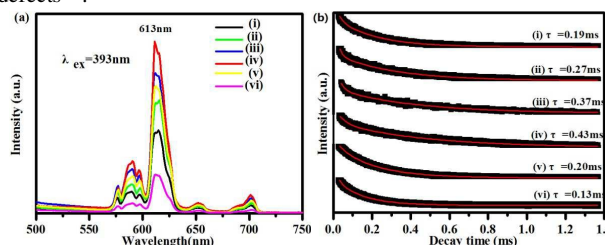


Fig.11 the emission spectra (a) and decay kinetics behaviors of $\text{SiO}_2:\text{xEu}^{3+}$ fibers for $x=0.04$ (i); $x=0.08$ (ii); $x=0.12$ (iii); $x=0.16$ (iv); $x=0.20$ (v); $x=0.24$ (vi)

Conclusions

In summary, a facile method that combines the advantages of both electrospinning technique and sol-gel process has been successfully developed to fabricate the one-dimensional $\text{SiO}_2:\text{Eu}^{3+}$ fibers luminescent materials with a relatively high Eu^{3+} ions concentration. The as-formed fibers present a smooth surface and uniform fiber-like morphology with a diameter about 660 nm when the composition of 16 mol% Eu^{3+} . Additionally, with the increasing of Eu^{3+} concentration, the diameters of fibers became wider, from nanoscale to microscale, which due to the increase of viscosity in precursor solution. Meanwhile, dendrimer PVP provided the driving force in the electrospinning process through the hydrogen bonding force with SiO_2 molecular. The results of XRD, FT-IR, XPS, EDS and the diffuse reflectance spectra indicated that Eu^{3+} ions doped into the SiO_2 fibers successfully and located at the interstitial sites of SiO_2 matrix by pseudo-covalent between Eu^{3+} ions and O ions by sharing with SiO_4 tetrahedral units,

which have effects on the band energy and symmetry of SiO₂ host. Under UV-light excitation, the obtained one-dimensional Eu³⁺ doped SiO₂ fibers showed strong characteristic red emission and the highest luminescent intensity was in the composition of up to 16 mol% Eu³⁺, the same as the longest lifetime, which is higher than other rare earth ions doped materials. Therefore, the obtained one-dimensional luminescent SiO₂:Eu³⁺ fibers is expected to broaden many potential types of applications on generating photonic devices (such as waveguides and amplifiers), lighting, biomedical engineering and color displays fields based on the good fluorescent properties and the advantages of SiO₂ matrix. Meanwhile, this method is very adaptable to other group IV elements fibers containing rare earth ions as well.

Acknowledgements

This present work was financially supported by the National Natural Science Foundation of China (21171066), the Key technology and equipment of efficient utilization of oil shale resources (No.OSR-05) and the Opening Research Funds Projects of the State Key Laboratory of Inorganic Synthesis and Preparative Chemistry and College of Chemistry, Jilin University (2016-01).

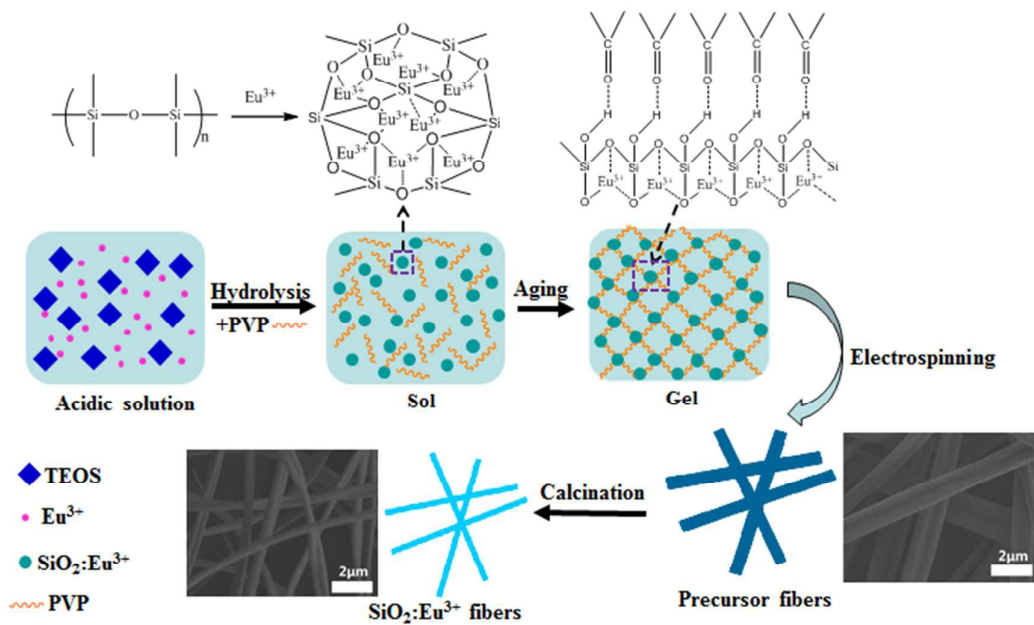
Notes and references

1. Y. Liu, D. Tu, H. Zhu and X. Chen, *Chemical Society Reviews*, 2013, **42**, 6924-6958.
2. L. Hu, R. Ma, T. C. Ozawa and T. Sasaki, *Angewandte Chemie*, 2009, **121**, 3904-3907.
3. H. Song, L. Yu, S. Lu, T. Wang, Z. Liu and L. Yang, *Applied Physics Letters*, 2004, **85**, 470.
4. J. Le Xie, C. X. Guo and C. M. Li, *Energy & Environmental Science*, 2014, **7**, 2559-2579.
5. N. G. Shang, U. Vetter, I. Gerhards, H. Hofsäuss, C. Ronning and M. Seibt, *Nanotechnology*, 2006, **17**, 3215.
6. H. B. Li, K. Y. Zheng, Y. Sheng, Y. H. Song, H. G. Zhang, J. Huang, Q. S. Huo and H. F. Zou, *Opt Laser Technol*, 2013, **49**, 33-37.
7. H. B. Zeng, X. W. Du, S. C. Singh, S. A. Kulinich, S. K. Yang, J. P. He and W. P. Cai, *Adv Funct Mater*, 2012, **22**, 1333-1353.
8. L. L. Wang, X. M. Liu, Z. Y. Hou, C. X. Li, P. P. Yang, Z. Y. Cheng, H. Z. Lian and J. Lin, *J Phys Chem C*, 2008, **112**, 18882-18888.
9. J. Y. Bai, R. F. Zhao, G. Han, Z. C. Li and G. W. Diao, *Rsc Adv*, 2015, **5**, 43328-43333.
10. X. Li, M. Yu, Z. Y. Hou, G. G. Li, P. A. Ma, W. X. Wang, Z. Y. Cheng and J. Lin, *J Solid State Chem*, 2011, **184**, 141-148.
11. Z. Y. Hou, C. X. Li, P. A. Ma, Z. Y. Cheng, X. J. Li, X. Zhang, Y. L. Dai, D. M. Yang, H. Z. Lian and J. Lin, *Adv Funct Mater*, 2012, **22**, 2713-2722.
12. R. Scotti, L. Conzatti, M. D'Arienzo, B. Di Credico, L. Giannini, T. Hanel, P. Stagnaro, A. Susanna, L. Tadiello and F. Morazzoni, *Polymer*, 2014, **55**, 1497-1506.
13. N. S. Swapna, M. Anantharaman, P. Joy, G. Mathew and K. Malini, 2015.
14. J. Wu and J. L. Coffey, *J Phys Chem C*, 2007, **111**, 16088-16091.
15. T. Uchino, A. Sakoh, M. Azuma, M. Takano, M. Takahashi and T. Yoko, *Journal of Physics: Condensed Matter*, 2002, **14**, 11111.
16. Y. Qiao, H. F. Chen, Y. Y. Lin, Z. Y. Yang, X. H. Cheng and J. B. Huang, *J Phys Chem C*, 2011, **115**, 7323-7330.
17. J. Wu and J. L. Coffey, *Chem Mater*, 2007, **19**, 6266-6276.
18. S. Banerjee and A. Datta, *Langmuir*, 2010, **26**, 1172-1176.
19. Z. Hou, Z. Cheng, G. Li, W. Wang, C. Peng, C. Li, P. a. Ma, D. Yang, X. Kang and J. Lin, *Nanoscale*, 2011, **3**, 1568-1574.
20. A. Mattos, G. Sombrio, M. Giroto, P. Franzen, R. Reis, M. Pereira and H. Boudinov, *Advanced Science, Engineering and Medicine*, 2014, **6**, 277-282.
21. Q. Z. Cui, X. T. Dong, J. X. Wang and M. Li, *J Rare Earth*, 2008, **26**, 664-669.
22. J.-H. He, *Thermal Science*, 2012, **16**, 327-330.
23. F. E. Ahmed, B. S. Lalia and R. Hashaikh, *Desalination*, 2015, **356**, 15-30.
24. Z. Hou, G. Li, H. Lian and J. Lin, *J Mater Chem*, 2012, **22**, 5254.
25. N. S. C. Zulkifli, I. Ab Rahman, D. Mohamad and A. Husein, *Ceramics International*, 2013, **39**, 4559-4567.
26. M. Tagaya, T. Ikoma, T. Yoshioka, S. Motozuka, Z. F. Xu, F. Minami and J. Tanaka, *J Colloid Interf Sci*, 2011, **363**, 456-464.
27. L. Y. Ren, T. J. Simmons, F. Y. Lu, O. Rahmi and S. P. Kotha, *Chem Eng J*, 2014, **254**, 39-45.
28. D. Kim, Y.-H. Jin, K.-W. Jeon, S. Kim, S.-J. Kim, O. H. Han, D.-K. Seo and J.-C. Park, *Rsc Adv*, 2015, **5**, 74790-74801.
29. M. Yan, H. F. Zou, H. Zhao, Y. H. Song, K. Y. Zheng, Y. Sheng, G. J. Wang and Q. S. Huo, *CrystEngComm*, 2014, **16**, 9216-9223.
30. T. Pirzada, S. A. Arvidson, C. D. Saquing, S. S. Shah and S. A. Khan, *Langmuir*, 2014, **30**, 15504-15513.
31. L. Wu, B. Wang, Y. Zhang, L. Li, H. R. Wang, H. Yi, Y. F. Kong and J. J. Xu, *Dalton T*, 2014, **43**, 13845-13851.
32. V. L. Chandraboss, B. Karthikeyan and S. Senthilvelan, *Physical Chemistry Chemical Physics*, 2015, **17**, 12100-12114.
33. M. L. Sun, Y. G. Su, C. F. Du, Q. H. Zhao and Z. L. Liu, *Rsc Adv*, 2014, **4**, 30820-30827.
34. C. J. Duan, A. C. A. Delsing and H. T. Hintzen, *Chem Mater*, 2009, **21**, 1010-1016.
35. F. Du, Y. Nakai, T. Tsuboi, Y. Huang and H. J. Seo, *J Mater Chem*, 2011, **21**, 4669-4678.
36. J. Chen, Y. Sheng, X. Zhou, F. Gao, C. Lin, Z. Shi, X. Xu and H. Zou, *Ceramics International*, 2015, **41**, 8552-8561.
37. L. F. Koao, H. C. Swart, R. I. Obed and F. B. Dejene, *J Lumin*, 2011, **131**, 1249-1254.
38. P. F. Du, L. X. Song, J. Xiong, H. B. Cao, Z. Q. Xi, S. Y. Guo, N. Y. Wang and J. J. Chen, *J Alloy Compd*, 2012, **540**, 179-183.
39. Y. Zhang, X. J. Li, D. L. Geng, M. M. Shang, H. Z. Lian, Z. Y. Cheng and J. Lin, *CrystEngComm*, 2014, **16**, 2196-2204.
40. Y. Zheng, H. You, G. Jia, K. Liu, Y. Song, M. Yang and H. Zhang, *Cryst Growth Des*, 2009, **9**, 5101-5107.

Journal Name

ARTICLE

41. Y. Gao, Y. Sun, H. Zou, Y. Sheng, X. Zhou, B. Zhang and B. Zhou, *Materials Science and Engineering: B*, 2016, **203**, 52-58.
42. L. L. Wang, Q. L. Wang, X. Y. Xu, J. Z. Li, L. B. Gao, W. K. Kang, J. S. Shi and J. Wang, *J Mater Chem C*, 2013, **1**, 8033-8040.



The formation mechanism of $\text{SiO}_2:\text{Eu}^{3+}$ fibers